
Article:
Mortazavi-Derazkola, S. orcid.org/0000-0002-1775-4525, Samadipour, M., Mohammadparast-Tabas, P. et al. (1 more author) (2025) Aesculus hippocastanum extract-mediated biosynthesis of silver-decorated zinc oxide nanoparticles and investigation of their photocatalytic, antibacterial, and antioxidant properties. Bioprocess and Biosystems Engineering. ISSN: 1615-7591

https://doi.org/10.1007/s00449-025-03193-7

Aesculus Hippocastanum extract-mediated biosynthesis of silver-decorated zinc oxide nanoparticles and investigation of their photocatalytic, antibacterial, and antioxidant properties

Sobhan Mortazavi-Derazkola[a], Maryam Samadipour[b], Pouria Mohammadparast-Tabas[b,c], Masoud Yousefi[d,*]

[a]*Medical Toxicology and Drug Abuse Research Center (MTDRC), Birjand University of Medical Sciences, Birjand, Iran*

[b]*Student Research Committee, Birjand University of Medical Sciences, Birjand, Iran*

[c]*Department of Medical Biotechnology, Faculty of Medicine, Birjand University of Medical Sciences, Birjand, Iran*

[d]*Department of Medical Microbiology, School of Medicine, Infectious Diseases Research Center, Birjand University of Medical Sciences, Birjand, Iran*

**Corresponding author email: masoud.yousefi164@gmail.com*

Abstract

In this research, silver-decorated zinc oxide nanoparticles (ZnO-Ag NPs) were fabricated using *Aesculus hippocastanum* fruit extract (ZnO-Ag@*AHFE* NPs), and their catalytic and antimicrobial properties were studied. The nanoparticles were identified using XRD, TEM, and FT-IR analyses, which confirmed their spherical morphology, uniform structure, and particle sizes ranging from 50 to 70 nm. The ZnO-Ag@*AHFE* NPs illustrated high antibacterial performance compared to the extract and ZnO NPs alone, achieving a minimum inhibitory concentration (MIC) of 125 µg/mL against *Escherichia coli* and *Pseudomonas aeruginosa*. Additionally, the ZnO-Ag@*AHFE* NPs exhibited outstanding photocatalytic efficiency, degrading methylene blue and rhodamine B dyes by 97.6% and 94.3%, respectively, surpassing the performance of other catalysts. Antioxidant assays revealed that the nanoparticles inhibited 85% of

DPPH free radicals, underscoring their potential in biological applications. This study presents a green method using *A. hippocastanum* fruit extract, offering an innovative approach to enhance the antibacterial, catalytic, and antioxidant properties of ZnO-Ag NPs. These findings highlight the transformative potential of green synthesis strategies for the development of multifunctional nanomaterials.

Keywords: *Aesculus Hippocastanum*; Antibacterial; Catalytic; Green synthesis; Silver; Zinc oxide.

1. Introduction

The emergence of antibiotic resistance among pathogenic bacteria in recent decades represents one of the most critical challenges facing human. This rise in resistant strains is largely attributed to the indiscriminate and excessive use of antibiotics [1]. Multidrug-resistant (MDR) bacteria, in particular, pose significant treatment challenges and are responsible for millions of deaths annually due to antibiotic-resistant infections. Projections suggest that, if current trends persist, antibiotic-resistant bacteria could lead to over 10 million deaths per year by 2050 [2]. As a result, the development of new antimicrobial agents capable of effectively targeting resistant bacterial strains remains an urgent and essential area of research.

Simultaneously, rapid industrialization has led to a marked increase in the generation of industrial wastewater, significantly contributing to environmental pollution [3]. Among the various contaminants, synthetic dyes are especially prevalent in effluents from textile, paper, leather, and cosmetics industries. These dyes not only compromise the aesthetic quality of water but also impede photosynthesis by obstructing light penetration [4]. Additionally, dyes pose toxic and hazardous threats to aquatic life and can cause allergies, itching, cancer, and mutagenesis in humans [5]. Methylene blue and rhodamine B are common dyes in industrial wastewater that are difficult to decompose due to their cyclic structures, making their removal from wastewater highly important [6]. Photocatalysis has emerged as a promising method for wastewater treatment, wherein pollutants are degraded in the presence of a photocatalyst and an energy

source [7]. Over the past decade a variety of nanomaterials Mn-ZnO [8], La-Doped WO_3 [9], Al–Fe/ZnO [10], Ni-doped ZnO [11], and ZnO-Ag [12] nanomaterials have been used to destroy pollutants.

Nanotechnology, as one of the most recent and transformative scientific advancements, has found applications across a wide range of fields. It has contributed significantly to progress in solar energy, waste management, sensor technology, medicine, and drug delivery systems [13-17]. At the nanoscale, materials exhibit unique physicochemical properties that differ markedly from their bulk counterparts, primarily due to their increased surface-to-volume ratio, which enhances their reactivity [18]. These characteristics make nanomaterials highly suitable for diverse applications. In the medical field, nanoparticles are employed for targeted drug delivery, diagnosis and treatment of diseases, wound healing, and antimicrobial agents [19]. Their nanoscale dimensions allow them to penetrate biological barriers, such as bacterial biofilms, which are typically resistant to conventional treatments [20]. Moreover, NPs can destroy bacteria through multiple mechanisms, making it difficult bacteria from developing resistance to them [21]. Beyond biomedical applications, nanoparticles are also extensively utilized in wastewater treatment facilities to remove a wide variety of pollutants [22].

Metal NPs possess notable antibacterial and photocatalytic properties, as demonstrated in numerous studies [23, 24]. Among these, zinc oxide (ZnO) has exhibited particularly strong photocatalytic activity [25]. Due to its low toxicity, ZnO has been approved by the U.S. Food and Drug Administration (FDA) and is widely used in sunscreen formulations as an effective ultraviolet light absorber [26].

Research has shown that incorporating metals into ZnO NPs can significantly enhance their antibacterial and photocatalytic properties [27]. Among various metals, silver is particularly notable for its potent antibacterial effects. It is widely employed as an antimicrobial agent in implants, coatings for medical and dental devices, and various topical formulations [28]. Several studies have demonstrated that decorating

ZnO NPs with silver markedly improves both their antibacterial efficacy and photocatalytic activity [29]. Accordingly, silver was selected for the decoration of ZnO NPs in the present study.

The synthesis method of NPs is a crucial component of nanotechnology. Broadly, NPs can be fabricated through chemical, physical, or green approaches. Chemical and physical assay include electrochemical, photochemical, sol-gel, hydrothermal, microwave-assisted, and ultrasound-assisted synthesis [30]. While these methods are effective, they often require sophisticated equipment, are time-consuming, and incur high costs. Moreover, the chemical reducing agents used in such methods may not be completely eliminated, posing potential risks to both human health and the environment [31]. Green synthesis has emerged as a sustainable and eco-friendly alternative. This approach utilizes plant extracts or microorganisms to produce nanoparticles, eliminating the need for specialized infrastructure and harmful reagents [32]. The use of natural extracts is particularly advantageous, as it enables faster reduction of metal ions and introduces plant-derived metabolites that can enhance the physicochemical properties of the synthesized nanoparticles [33].

The *Aesculus hippocastanum* (commonly referred to as *A. hippocastanum*), belongs to the *Hippocastanaceae* family. It is considered one of the most prominent and valuable native tree species in Southeastern Europe and is also found in temperate regions of Asia, including the Indian subcontinent, the Himalayas, and surrounding areas [34]. The tree produces numerous seeds, approximately 3.5 cm in diameter, which are shiny brown and encased in a hard capsule [35]. *A. hippocastanum* seeds contain high concentrations of saponin, escin, and coumarin glycosides, which have antithrombotic effects and medicinal applications [36]. Traditionally, *A. hippocastanum* seeds have been used to prevent and treat a range of conditions, including venous congestion in the legs, bruising, arthritis, rheumatism, and diarrhea [37].

Herein, we report a green, one-pot synthesis of silver-decorated zinc oxide nanoparticles using *Aesculus hippocastanum* fruit extract. This work is distinguished by its use of a novel plant-mediated approach that is both eco-friendly and cost-effective, eliminating the need for hazardous chemicals. Importantly, the resulting nanomaterials exhibit enhanced antibacterial, antioxidant, and photocatalytic activities compared to ZnO or Ag nanoparticles synthesized through conventional methods. The synergistic effects observed suggest promising applications in environmental remediation and biomedical fields, marking a significant advancement in the development of multifunctional nanomaterials through sustainable green chemistry.

2. Experimental

2.1. Materials

In this study, $Zn(NO_3)_2.6H_2O$ (98%) and $AgNO_3$ (≥99.9%; Sigma Aldrich) were used for NPs synthesis. PVA (polyvinyl alcohol; 98%) and NaOH was purchased from Sigma-Aldrich Company. Methanol (Dr. Mojallali Co., Iran) was employed for extraction. Five strains were purchased from the Pasteur Institute (Iran) and tested including *Staphylococcus aureus* (*S. aureus*, ATCC 29213), *Escherichia coli* (*E. coli*, ATCC 25922), *Pseudomonas aeruginosa* (*P. aeruginosa*, ATCC 27853), *Klebsiella pneumoniae* (*K. pneumoniae*, ATCC 9997), and *Enterococcus faecalis* (*E. faecalis*, ATCC 29212). Additionally, the antioxidant test was performed using the 2,2-diphenyl-1-picrylhydrazyl (DPPH) kit from Zantox kits (Kavosh Arian Azma Co., Iran). All experiments, including antibacterial, antioxidant, and photocatalytic tests, were carried out in triplicate to ensure reproducibility and reliability of the results.

2.2. Preparation of Aesculus hippocastanum fruit extract

The aqueous extraction method was used for extraction. *A. hippocastanum* fruit was collected from the western regions of the country (Iran) and confirmed by a botanist. After washing, the dried kernel (flesh) of *A. hippocastanum* fruit was ground. To extract, 100 g of *A. hippocastanum* fruit powder was mixed with

one liter of water and placed in a water bath at 80°C. The extract was then filtered using filter paper and dried using a freeze dryer.

2.3. Fabrication of ZnO NPs

One gram of PVA as a surfactant was added in 50 mL of distilled water at 60°C on a stirrer until the solution became transparent. In another beaker, zinc nitrate was dissolved in distilled water under stirring. The PVA solution was then slowly added to the zinc nitrate solution while stirring. After 20 min, NaOH solution (1M) was added dropwise until the pH reached 12, turning the suspension milky. The mixture was stirred for 120 min, and then centrifuged and washed. This washing and centrifugation removed the surfactant and excess ions. The remaining sediment was dried at 60°C for 24 h, and then calcined in an oven at 450°C for 3 h, resulting in ZnO NPs.

2.4. Bio-fabrication of ZnO-Ag@AHFE NPs

In this study, ZnO-Ag NPs were fabricated using a green process with *A. hippocastanum* fruit extract. To synthesize ZnO-Ag@*AHFE* NPs, 100 mg of ZnONPs obtained in the previous step were sonicated in a solution of water and ethanol in a ratio of 2:1 to create a uniform suspension. The mixture was then stirred. Separately, silver nitrate (10% mol) was added in 10 mL of distilled water and added dropwise to the ZnO suspension. Concurrently, 100 mg of *A. hippocastanum* fruit extract was added in 10 mL of distilled water, and its pH was adjusted to 12 using NaOH (1 M). After filtering, the extract was added dropwise to the ZnO and silver nitrate suspension. The color change to dark indicated the fabrication of silver NPs on the surface of ZnO NPs. After 90 min, the precipitate was centrifuged and washed (Fig.1). In a study conducted by Dridi et al. on *A. hippocastanum* extract, it was determined that quercetin is the predominant active compound. Based on their findings [38], we designed the proposed mechanism for the formation of ZnO-Ag@*AHFE* NPs, as illustrated in Scheme.1.

2.5. Examination of Antibacterial property

This study was conducted on five standard bacterial strains including *E. coli, K. pneumoniae*, and *P. aeruginosa*, *S. aureus*, and *E. faecalis*. To test antibacterial performance of ZnONPs, ZnO-Ag@*AHFE* NPs, and *A. hippocastanum* fruit extract, 100 µl of Mueller Hinton broth (Merck Co., Germany) containing different concentrations of the compounds under study was dispensed into the wells of a 96-well plate. Subsequently, 100 µl of a bacterial suspension (10^6 CFU/mL) was added to each well of the plates. In the experiment, the positive and negative controls were established by combining a bacterial suspension with the medium for the positive control, and by using only the culture medium for the negative control. Finally, the lowest concentration of the substances that showed no turbidity in the wells was recorded as the MIC for the products. Furthermore, tetracycline was employed as a potent antibacterial agent to serve as a reference for evaluating the antibacterial activity of the tested compounds.

2.6. Examination of antioxidant property

The antioxidant performance of ZnO NPs, ZnO-Ag@*AHFE* NPs, and *A. hippocastanum* fruit extract were evaluated using the DPPH assay. This method measures the inhibition of the DPPH free radical. In brief, 10 µl of samples at various concentrations were added to the wells of a 96-well plate. Subsequently, 250 µl of purple DPPH solution was added to each well. After incubation (15 min), the absorbance was read at 517 nm. DPPH free radical exhibits absorbance at 517 nm; however, upon reaction with substances possessing antioxidant properties, it is reduced, and its color changes from purple to yellow, resulting in a decrease in absorbance at 517 nm. Thus, materials with higher antioxidant properties will reduce the color intensity to a greater extent. The percentage of DPPH free radical inhibition was measured using the following formula:

$$\frac{\mathrm{OD_{Blank}} - \mathrm{OD_{Sample}}}{\mathrm{OD_{Blank}}} \times 100 \;=\; \text{Inhibition } (\%) \qquad (1)$$

Where OD_{Blank} is the absorbance of the control (without sample), and OD_{Sample} is the absorbance of the sample. Results are presented as mean ± standard deviation (SD).

2.7. Investigation of photocatalytic performance

The photocatalytic performance of ZnO NPs and ZnO-Ag@*AHFE* NPs in the removal of rhodamine B and methylene blue dyes was evaluated. A 10 mg/L solution of each dye was prepared and poured into a quartz tube, chosen due to its high transparency in the UV region, ensuring that the UV-400 light effectively reaches the photocatalyst. A specific amount of NPs was added to the dye solution, and the resulting suspension was stirred for 30 min in the dark with aeration to balance adsorption and desorption. The contents of the quartz tube were then exposed to UV-400 light with continuous stirring and aeration. At specific intervals during the irradiation period, samples were taken and centrifuged at 10000 rpm to separate the nanoparticles from the solution. The clear supernatant was then collected and analyzed using a UV/Vis spectrophotometer at wavelengths corresponding to rhodamine B and methylene blue. This step ensured that no suspended nanoparticles interfered with the absorbance measurements. The pollutant degradation during the photocatalytic process was calculated using the formula:

$$\text{Degradation } (\%) = \frac{C_0 - C_t}{C_0} \times 100 \quad (2)$$

Where C_0 is the initial absorbance, and C_t is the absorbance at time t.

2.8. Characterization

To confirm the synthesis of ZnONPs and ZnO-Ag@*AHFE* NPs, X-ray diffraction (XRD; Philips PW1800 with CuKa radiation) analysis was performed. Fourier-transform infrared spectroscopy (FT-IR) analysis was conducted using PerkinElmer Spectrum Two™ IR spectrometer; Model L160000U. The FT-IR spectra were obtained using the KBr pellet method. By identifying different functional groups, the

presence of extract-derived functional groups in the synthesized nanoparticles was confirmed by comparing the spectra of the products. The shape of the products was determined using images obtained from Transmission Electron Microscopy (TEM; Zeiss-EM10C-100 KV).

3. Results and Discussion

3.1. XRD patterns

XRD analysis was conducted to confirm the synthesis of ZnONPs and ZnO-Ag@*AHFE* NPs. The XRD patterns for these samples are presented in Figures 2. The XRD pattern of ZnO NPs (Fig. 2a) shows eleven distinct peaks that align with the standard diffraction pattern of zinc oxide (JCPDS 01-080-0075) [39]. These peaks at 2θ angles of 31.56°, 34.54°, 36.17°, 47.67°, 56.39°, 62.13°, 66.19°, 67.22°, 69.45°, 72.61°, and 77.57° correspond to the (100), (002), (101), (102), (110), (103), (200), (112), (201), (004), and (202). These results are consistent with the XRD patterns reported by *Chitradevi* et al., who observed similar peaks at 2θ angles of 31.08°, 34.05°, 36.03°, 47.08°, 56.08°, 63.09°, 67.09°, 69.01°, 72.03°, and 77.01° [39]. The resulting XRD pattern (related to ZnO-Ag@*AHFE* NPs) shows peaks that match both the standard diffraction patterns of zinc oxide and silver (JCPDS 01-087-0717) [40], indicating the successful synthesis of ZnO-Ag@*AHFE* NPs. In addition to the eleven peaks corresponding to ZnO, three additional peaks at 2θ angles of 38.23°, 44.58°, and 77.41° were observed (Fig.2b), corresponding to the Miller indices (111), (200), and (311) of silver. These additional peaks align with the findings of *Rafique* et al., who observed similar peaks at 38.37°, 44.78°, and 64.80° in their synthesis of ZnO-Ag NPs [41]. A comparison of the XRD patterns of ZnO NPs and ZnO-Ag@*AHFE* NPs reveals a decrease in peak intensity in the ZnO-Ag@*AHFE* NPs compared to the ZnO NPs. This reduction in intensity is attributed to the incorporation of silver NPs onto the ZnO NPs. No additional peaks were observed, confirming the high purity of the synthesized NPs. The reduction in the intensity of XRD peaks after the deposition of

nanoparticles on the substrate has been reported in various studies [42, 43]. The crystalline size of the products was determined using the Debye-Scherrer equation [44]. The crystalline sizes were found to be 44.2 nm for ZnO NPs and 56.3 nm for ZnO-Ag@*AHFE* NPs.

3.2. FT-IR spectra

The FT-IR spectra of ZnO NPs and ZnO-Ag@*AHFE* NPs are depicted in Figure 3. The FT-IR spectrum of ZnO NPs exhibits a prominent absorption band at 479 cm^{-1}, indicating the presence of a metal-oxygen bond in ZnO NPs. This peak confirms the formation of the Zn-O bond between zinc and oxygen in the ZnO structure [45]. The FT-IR spectrum of Ag-decorated ZnO synthesized using *A. hippocastanum* fruit extract reveals several characteristic peaks corresponding to various functional groups in the extract. Notable peaks include 3374 cm^{-1} (OH stretch), 2941 cm^{-1} (C-H stretch), 1623 cm^{-1} (C=O bond), 1462 cm^{-1} (C-H bending), and 1087 cm^{-1} (C-O stretch). The FT-IR spectrum of ZnO-Ag@*AHFE* NPs shows peaks similar to those observed in the *A. hippocastanum* fruit extract spectra. The metal-oxygen bond peak is present but less intense compared to the ZnO NPs, likely due to the interference caused by silver incorporation. Other peaks in the ZnO-Ag@*AHFE* NPs spectrum align with those observed in the *A. hippocastanum* fruit extract spectrum, confirming the presence of extract-derived functional groups in the ZnO-Ag NPs. This observation indicates that the *A. hippocastanum* fruit extract is on the surface of the ZnO-Ag NPs. Jakinala et al. reported similar findings in the FT-IR spectra of *Stenotaphrum secundatum* extracts, noting functional groups such as alkyl C-O bonds, C-N bonds, and C-H stretching, which are analogous to those observed in our study for ZnO-Ag NPs synthesized with *A. hippocastanum* fruit extract. This consistency reinforces the incorporation of plant extract-derived functional groups in the synthesized nanoparticles [46].

3.3. TEM analysis

TEM was employed to examine the morphology, particle size, and structural features of the synthesized ZnO-Ag@*AHFE* NPs. The TEM images (Fig. 4) reveal that the nanoparticles are predominantly spherical in shape and exhibit a relatively uniform distribution. The average particle size was estimated to be in the range of approximately 50-70 nm, which is consistent with nanoscale dimensions and supports the successful synthesis of the desired nanostructure. Furthermore, the images display small, well-dispersed dark spots distributed on the surface of the ZnO nanoparticles. These features are attributed to the presence of silver nanoparticles, indicating the successful decoration of ZnO with Ag. The contrast observed in the TEM images between the ZnO matrix and the smaller Ag particles suggests effective attachment without significant aggregation. Notably, no thick organic coating was observed around the nanoparticles, implying a relatively low amount of surface-bound phytocompounds derived from the *Aesculus hippocastanum* fruit extract [43]. However, the presence of these organic capping agents is further confirmed through FTIR analysis (Section 3.2), which reveals characteristic functional groups from the plant extract.

3.4. Antibacterial property

The antibacterial properties of A. hippocastanum fruit extract, ZnO NPs, and ZnO-Ag@*AHFE* NPs were evaluated. The results of this test are presented in Table 1. As shown in the table, the *A. hippocastanum* fruit extract, up to a concentration of 15,000 µg/mL, could only prevent the growth of *E. faecalis* bacteria and had no effect on the other tested strains. Next, the antibacterial property of ZnO NPs was measured. The results showed that ZnONPs affected all the tested strains and inhibited their growth at the concentrations used. These NPs had the most significant effect on *S. aureus* bacteria, preventing growth at a concentration of 500 µg/mL, and had the least effect on *P. aeruginosa* and *E. faecalis* bacteria (MIC = 4000 µg/mL). Finally, the antibacterial property of ZnO-Ag@*AHFE* NPs was investigated. The results indicated that ZnO-Ag@*AHFE* NPs exhibited the strongest antibacterial properties among the compounds evaluated. ZnO-Ag@*AHFE* NPs showed more antibacterial effects on Gram-negative bacteria than on

Gram-positive bacteria. Specifically, these NPs had the greatest effect on Gram-negative strains of *E. coli* (MIC = 125 µg/mL) and *P. aeruginosa* (MIC = 125 µg/mL), and the least effect on the Gram-positive bacterium *E. faecalis* (MIC = 750 µg/mL). The antibacterial results of the nanoparticles were compared with those of tetracycline, as reported in our previous study [47] and presented in Table 1. The presence of silver NPs enhanced the antibacterial properties of ZnO-Ag@*AHFE* NPs compared to ZnONPs alone. This study found that decorating ZnO-NPs with silver NPs significantly increased their antibacterial properties. To facilitate better comparison of antimicrobial activity among different samples, a bar graph was plotted, as shown in Figure 5. Similar results were observed in studies conducted by *Sali* et al. [48] and *Thatikayala* et al. [49]. In the study by *Khan* et al., it was also observed that decorating ZnONPs with silver increased their antibacterial properties, and as the percentage of silver NPs increased, so did the antibacterial efficacy [50]. In the current study, ZnO-Ag@*AHFE* NPs were found to have more pronounced antibacterial effects on Gram-negative bacteria than on Gram-positive bacteria. Studies by *Noohpisheh* et al. and *Kiani* et al. also observed that NPs exhibit stronger antibacterial effects on Gram-negative bacteria. This difference is attributed to the structural differences in the cell walls of these bacteria [51, 52]. Gram-negative strain has a thinner cell wall compared to Gram-positive strain, making it easier for NPs to penetrate. Additionally, Gram-negative bacteria possess a lipopolysaccharide layer with a negative charge, which facilitates the absorption and accumulation of NPs on their surface, ultimately leading to their destruction [51, 53]. The precise antibacterial mechanism of NPs is not fully understood, but studies suggest that NPs cause bacterial dysfunction and destruction through multiple pathways (Figure 6). Initially, NPs adhere to the bacterial surface, leading to oxidative stress, metal ion release, and membrane disruption. This disruption allows NPs to enter the bacteria and causes the release of intracellular contents [48]. Inside the bacteria, NPs can damage proteins, DNA, and enzymes, leading to disturbances in vital functions such as metabolic enzyme activity, replication, transcription, and translation [54, 55]. The increased oxidative stress further disrupts

bacterial functions [56]. Ultimately, the combined effects of membrane disruption, release of intracellular materials, and loss of membrane integrity result in bacterial destruction.

3.5. Antioxidant activity

Free radicals are among the most dangerous intracellular substances due to their high reactivity with various cellular components, causing significant damage. Normally, cells neutralize free radicals through antioxidant systems, preventing harm to vital molecules [57]. Oxidative stress arises when the generation of free radicals surpasses the cell's ability to neutralize them. This imbalance can result in cellular damage and contribute to the development of diseases [58]. Substances with antioxidant properties can prevent cell damage by neutralizing free radicals [59]. In this study, the antioxidant activities of ZnO NPs, ZnO-Ag@*AHFE* NPs, and *A. hippocastanum* fruit extract were assessed using the DPPH free radical scavenging assay. The results, presented in Table 2, indicate that ZnO NPs exhibited the lowest antioxidant activity, inhibiting 8 ± 0.6 % of DPPH free radicals at a concentration of 4 mg/mL. In comparison, *A. hippocastanum* fruit extract inhibited 35 ± 2.1 % of DPPH free radicals at the same concentration, which can be attributed to the presence of phenolic compounds [60]. *Kedzierski* et al. demonstrated that *A. hippocastanum* seed extract could inhibit 80% of DPPH free radicals at a concentration of 10 mg/mL [61]. ZnO-Ag@*AHFE* NPs showed the highest antioxidant properties among the tested compounds, inhibiting 85 ± 2.4 % of DPPH free radicals at a concentration of 2 mg/mL. Silver is known for its intrinsic antioxidant properties, as evidenced by studies from *Bedlovicova* et al. and *Keshari* et al., which highlighted the significant antioxidant properties of silver NPs [62, 63]. *Hameed* et al. found that ZnO NPs decorated with silver had greater antioxidant activity than ZnONPs alone [64]. *Suresh* et al. observed that ZnO NPs decorated with silver at a concentration of 0.5 mg/mL could inhibit 62% of DPPH free radicals [65].

3.6. Photocatalytic activity

The photocatalytic degradation results of two dyes indicated that, in the absence of nanoparticles, dye removal was negligible. This suggests that the presence of NPs in the suspension plays an essential role in dye degradation under light irradiation. The degradation performance of ZnO NPs (Fig. 7) revealed that they were capable of removing approximately 84.1% of rhodamine B and 75.2% of methylene blue under the tested conditions. To evaluate the influence of silver incorporation, ZnO-Ag@*AHFE* NPs were evaluated over the same period (Fig. 8). The results demonstrated an enhanced photocatalytic performance, with degradation efficiencies reaching 94.3% for rhodamine B and 97.6% for methylene blue. This improvement may be attributed to the presence of silver, which could enhance charge separation or surface reactivity, although the exact mechanism remains subject to further investigation. Previous studies have reported that decorating ZnO with noble metals such as silver can improve photocatalytic activity [49]. For instance, Hosny et al. observed similar improvements with silver-modified ZnO [66]. Stanley et al. reported that Ag-decorated ZnO could remove up to ~98% of methylene blue under similar conditions [67]. Ahmad et al. also noted that ZnO NPs alone removed around 75% of rhodamine B, whereas Ag-decorated ZnO achieved degradation up to 91% [68], which is consistent with the present findings.

4. Conclusion

This research successfully developed ZnO-Ag NPs through a green approach using *A. hippocastanum* fruit extract. The fabricated nanoparticles exhibited remarkable multifunctional properties, including potent antibacterial effects, 85% DPPH radical scavenging activity, and impressive photocatalytic performance, achieving 97.6% degradation of methylene blue and 94.3% of rhodamine B. These findings underscore the potential of ZnO-Ag NPs in medical, environmental, and industrial fields, emphasizing the benefits of green synthesis in creating efficient nanoparticles.

Acknowledgment

This research is the result of research with ethical codeIR.BUMS.REC.1400.365. We are grateful to Birjand University of Medical Sciences for supporting this research (Grant No. 456546).

References

[1] M. Frieri, K. Kumar, A. Boutin, Antibiotic resistance, Journal of Infection and Public Health, 10 (2017) 369-378.

[2] E. Banin, D. Hughes, O.P. Kuipers, Editorial: Bacterial pathogens, antibiotics and antibiotic resistance, FEMS Microbiology Reviews, 41 (2017) 450-452.

[3] F.H. Abdullah, N.H.H.A. Bakar, M.A. Bakar, Current advancements on the fabrication, modification, and industrial application of zinc oxide as photocatalyst in the removal of organic and inorganic contaminants in aquatic systems, Journal of Hazardous Materials, 424 (2022) 127416.

[4] A. Rafiq, M. Ikram, S. Ali, F. Niaz, M. Khan, Q. Khan, M. Maqbool, Photocatalytic degradation of dyes using semiconductor photocatalysts to clean industrial water pollution, Journal of Industrial and Engineering Chemistry, 97 (2021) 111-128.

[5] A. Akbari, Z. Sabouri, H.A. Hosseini, A. Hashemzadeh, M. Khatami, M. Darroudi, Effect of nickel oxide nanoparticles as a photocatalyst in dyes degradation and evaluation of effective parameters in their removal from aqueous environments, Inorganic Chemistry Communications, 115 (2020) 107867.

[6] P.A. Luque, H.E. Garrafa-Gálvez, O. Nava, A. Olivas, M.E. Martínez-Rosas, A.R. Vilchis-Nestor, A. Villegas-Fuentes, M.J. Chinchillas-Chinchillas, Efficient sunlight and UV photocatalytic degradation of Methyl Orange, Methylene Blue and Rhodamine B, using Citrus×paradisi synthesized SnO2 semiconductor nanoparticles, Ceramics International, 47 (2021) 23861-23874.

[7] A.K. Sibhatu, G.K. Weldegebrieal, S. Sagadevan, N.N. Tran, V. Hessel, Photocatalytic activity of CuO nanoparticles for organic and inorganic pollutants removal in wastewater remediation, Chemosphere, 300 (2022) 134623.

[8] T. Iqbal, M. Afzal, B.A. Al- Asbahi, S. Afsheen, I. Maryam, A. Mushtaq, S. Kausar, A. Ashraf, Enhancing apple shelf life: A comparative analysis of photocatalytic activity in pure and manganese-doped ZnO nanoparticles, Materials Science in Semiconductor Processing, 173 (2024) 108152.

[9] T. Iqbal, R.M. Munir, A. Younas, S. Afsheen, M.S. Mansha, S. Ahsan, A.A. AlObaid, N. Al-Zaqri, Facile Green Synthesis of La-Doped WO3 Nanomaterials for Their Photocatalytic Activity against Hazardous Pharmaceutical Compounds: Experimental and COMSOL Simulation, Journal of Inorganic and Organometallic Polymers and Materials, 34 (2024) 3300-3313.

[10] N.R. Khalid, A. Hammad, M.B. Tahir, M. Rafique, T. Iqbal, G. Nabi, M.K. Hussain, Enhanced photocatalytic activity of Al and Fe co-doped ZnO nanorods for methylene blue degradation, Ceramics International, 45 (2019) 21430-21435.

[11] M.I. Khan, N. Fatima, M. Shakil, M.B. Tahir, K.N. Riaz, M. Rafique, T. Iqbal, K. Mahmood, Investigation of in-vitro antibacterial and seed germination properties of green synthesized pure and nickel doped ZnO nanoparticles, Physica B: Condensed Matter, 601 (2021) 412563.

[12] S. Mohammadi-Aghdam, F. Bahraini, S.M. Ghoreishi, In-vitro anticancer on acute lymphoblastic leukemia NALM-6 cell line, antibacterial and catalytic performance of eco-friendly synthesized ZnO and Ag-doped ZnO nanoparticles using Hedera colchica extract, Biomass Conversion and Biorefinery, 14 (2024) 20037-20052.

[13] J. Zhao, Q. Shao, S. Ge, J. Zhang, J. Lin, D. Cao, S. Wu, M. Dong, Z. Guo, Advances in Template Prepared Nano-Oxides and their Applications: Polluted Water Treatment, Energy, Sensing and Biomedical Drug Delivery, The Chemical Record, 20 (2020) 710-729.

[14] M.S. Ardestani, Z. Zaheri, P. Mohammadzadeh, A. Bitarafan-Rajabi, S.M. Ghoreishi, Novel manganese carbon quantum dots as a nano-probe: Facile synthesis, characterization and their application in naproxen delivery (Mn/CQD/SiO2@naproxen), Bioorganic Chemistry, 115 (2021) 105211.

[15] A. Ebrahimi, M. Pirali Hamedani, P. Mohammadzadeh, M. Safari, S. Esmaeil Sadat Ebrahimi, M. Seyed Hamzeh, M. Shafiee Ardestani, S. Masoumeh Ghoreishi, 99mTc- Anionic dendrimer targeted vascular endothelial growth factor as a novel nano-radiotracer for in-vivo breast cancer imaging, Bioorganic Chemistry, 128 (2022) 106085.

[16] B. davoodikia, M. Pirali Hamedani, M. Saffari, S. Esmaeil Sadat Ebrahimi, M. Seyyed hamzeh, S. Hashemi, M. Shafiee Ardestani, S. Masoumeh Ghoreishi, Synthesis of novel nano-radiotracer for in-vivo bone imaging: 99mTc- citric acid based PEG dendrimer and its conjugation with alendronate, Arabian Journal of Chemistry, 15 (2022) 104060.

[17] A.S. Helal, M. Hémadi, J.S. Lomas, S. Ammar, A. Abdelhafiz, S.M. El-Sheikh, S.M. Sheta, M. Galanek, M.H. Hassan, J.-K. Chang, J. Li, Uranium removal from environmental water and nuclear waste: Nanomaterial solutions and their environmental sustainability, Chemical Engineering Journal, 507 (2025) 160298.

[18] N. Joudeh, D. Linke, Nanoparticle classification, physicochemical properties, characterization, and applications: a comprehensive review for biologists, Journal of Nanobiotechnology, 20 (2022) 262.

[19] S. Vijayaram, H. Razafindralambo, Y.-Z. Sun, S. Vasantharaj, H. Ghafarifarsani, S.H. Hoseinifar, M. Raeeszadeh, Applications of Green Synthesized Metal Nanoparticles — a Review, Biological Trace Element Research, 202 (2024) 360-386.

[20] A.S. Joshi, P. Singh, I. Mijakovic, Interactions of Gold and Silver Nanoparticles with Bacterial Biofilms: Molecular Interactions behind Inhibition and Resistance, International Journal of Molecular Sciences, 21 (2020) 7658.

[21] M.F. Gómez-Núñez, M. Castillo-López, F. Sevilla-Castillo, O.J. Roque-Reyes, F. Romero-Lechuga, D.I. Medina-Santos, R. Martínez-Daniel, A.N. Peón, Nanoparticle-Based Devices in the Control of Antibiotic Resistant Bacteria, Front Microbiol, 2020, pp. 563821.

[22] A.K. Al-Buriahi, A.A. Al-Gheethi, P. Senthil Kumar, R.M.S. Radin Mohamed, H. Yusof, A.F. Alshalif, N.A. Khalifa, Elimination of rhodamine B from textile wastewater using nanoparticle photocatalysts: A review for sustainable approaches, Chemosphere, 287 (2022) 132162.

[23] J. Zhang, W. Wang, S. Huang, Y. Lv, M. Li, M. Wu, H. Wang, Metal-free photocatalyst with reduced graphene oxide-doped graphitic carbon nitride homojunctions for efficient antibacterial applications††Electronic supplementary information (ESI) available. See DOI: https://doi.org/10.1039/d4ra07829b, RSC Advances, 15 (2025) 2444-2451.

[24] H. Chen, D. Li, Y. Zheng, K. Wang, X. Zhang, S. Zhou, S. Wei, F. Yong, J. Nie, H. Wen, J. Wu, W. Xue, S. Huang, Metal-free carbon-dots nanozyme with oxidase-like activity as photocatalysts for highly efficient detection/reduction of Cr(VI) and antibacterial application, Separation and Purification Technology, 356 (2025) 129852.

[25] V.P. Klienchen de Maria, F.F. Guedes de Paiva, J.R. Tamashiro, L.H.P. Silva, G. da Silva Pinho, F. Rubio-Marcos, A. Kinoshita, Advances in ZnO nanoparticles in building material: Antimicrobial and photocatalytic applications – Systematic literature review, Construction and Building Materials, 417 (2024) 135337.

[26] F. Sofaturrohman, L. Rifka, M. Syalsabilla, M. Syuriyani, N. Raisa, R. Jonuarti, R. Hidayat, Analysis Titanium Dioxide and Zinc Oxide in Physical Sunscreen Commercial with Protection Value 35 SPF, PILLAR OF PHYSICS, 17 (2024).

[27] A. Muhammed, T.G. Asere, T.F. Diriba, Photocatalytic and Antimicrobial Properties of ZnO and Mg-Doped ZnO Nanoparticles Synthesized Using Lupinus albus Leaf Extract, ACS Omega, 9 (2024) 2480-2490.

[28] I.X. Yin, J. Zhang, I.S. Zhao, M.L. Mei, Q. Li, C.H. Chu, The Antibacterial Mechanism of Silver Nanoparticles and Its Application in Dentistry, International Journal of Nanomedicine, 15 (2020) 2555-2562.

[29] R. Rajendran, A. Mani, Photocatalytic, antibacterial and anticancer activity of silver-doped zinc oxide nanoparticles, Journal of Saudi Chemical Society, 24 (2020) 1010-1024.

[30] O. Pryshchepa, P. Pomastowski, B. Buszewski, Silver nanoparticles: Synthesis, investigation techniques, and properties, Advances in Colloid and Interface Science, 284 (2020) 102246.

[31] A. Mukherjee, D. Sarkar, S. Sasmal, A review of green synthesis of metal nanoparticles using algae, Front Microbiol, 12 (2021) 693899.

[32] S. Ying, Z. Guan, P.C. Ofoegbu, P. Clubb, C. Rico, F. He, J. Hong, Green synthesis of nanoparticles: Current developments and limitations, Environmental Technology & Innovation, 26 (2022) 102336.

[33] P.K. Dikshit, J. Kumar, A.K. Das, S. Sadhu, S. Sharma, S. Singh, P.K. Gupta, B.S. Kim, Green Synthesis of Metallic Nanoparticles: Applications and Limitations, Catalysts, 11 (2021) 902.

[34] J. Čukanović, V. Tešević, M. Jadranin, M. Ljubojević, E. Mladenović, S. Kostić, Horse chestnut (Aesculus hippocastanum L.) seed fatty acids, flavonoids and heavy metals plasticity to different urban environments, Biochemical Systematics and Ecology, 89 (2020) 103980.

[35] S.I. Rafiq, K. Jan, S. Singh, D.C. Saxena, Physicochemical, pasting, rheological, thermal and morphological properties of horse chestnut starch, Journal of Food Science and Technology, 52 (2015) 5651-5660.

[36] T. Takahashi, Y. Tsurunaga, W.F. Schmidt, K. Yoshino, Functional evaluation of horse chestnut seed and its application in the production of compounded paper for effective utilization of an untapped resource, Journal of Wood Science, 63 (2017) 484-495.

[37] S. Idris, A. Mishra, M. Khushtar, Phytochemical, ethanomedicinal and pharmacological applications of escin from Aesculus hippocastanum L. towards future medicine, Journal of Basic and Clinical Physiology and Pharmacology, 31 (2020).

[38] A. Dridi, F.S. Reis, T.C.S.P. Pires, R.C. Calhelha, C. Pereira, K. Zaghdoudi, I.C.F.R. Ferreira, L. Barros, J.C.M. Barreira, Aesculus hippocastanum L.: A Simple Ornamental Plant or a Source of Compelling Molecules for Industry?, Separations, 10 (2023) 160.

[39] T. Chitradevi, A. Jestin Lenus, N. Victor Jaya, Structure, morphology and luminescence properties of sol-gel method synthesized pure and Ag-doped ZnO nanoparticles, Materials Research Express, 7 (2020) 015011.

[40] M.E. Taghavizadeh Yazdi, M. Darroudi, M.S. Amiri, H. Zarrinfar, H.A. Hosseini, M. Mashreghi, H. Mozafarri, A. Ghorbani, S.H. Mousavi, Antimycobacterial, Anticancer, Antioxidant and Photocatalytic Activity of Biosynthesized Silver Nanoparticles Using Berberis Integerrima, Iranian Journal of Science and Technology, Transactions A: Science, 46 (2022) 1-11.

[41] S. Rafique, S. Bashir, R. Akram, S. Jawaid, M. Bashir, A. Aftab, A. Attique, S.U. Awan, In vitro anticancer activity and comparative green synthesis of ZnO/Ag nanoparticles by moringa oleifera, mentha piperita, and citrus lemon, Ceramics International, 49 (2023) 5613-5620.

[42] M. Siami-Aliabad, E. Chamani, S. Mortazavi-Derazkola, Z. Khanjari, Z. Kiani, H. Aramjoo, A. Rezaei Farimani, P.N. Dang, M. Fattahi, Bimetallic S. pachycarpa@Ag-doped ZnO alloy nanoparticles unveil therapeutic promise: Revolutionizing multiple myeloma treatment, Journal of Alloys and Compounds, 975 (2024) 172986.

[43] Z. Kiani, S. Mirjalili, K. Heydaryan, P. Mohammadparast, H. Aramjoo, F. Bahraini, A. Yousefinia, M. Torabi, S.M. Ghoreishi, M. Fattahi, S. Mortazavi-Derazkola, Harmonizing nature and nanotechnology: Phytoextract-mediated synthesis of Ag-doped ZnO nanoparticles using Lavandula

stoechas extract for environmental and biomedical applications, Journal of Drug Delivery Science and Technology, 96 (2024) 105708.

[44] S. Mortazavi-Derazkola, M. Reza Naimi-Jamal, S. Masoumeh Ghoreishi, Synthesis, Characterization, and Atenolol Delivery Application of Functionalized Mesoporous Hydroxyapatite Nanoparticles Prepared by Microwave-Assisted Co-precipitation Method, Current Drug Delivery, 13 (2016) 1123-1129.

[45] R. Mohammadzadeh Kakhki, R. Tayebee, F. Ahsani, New and highly efficient Ag doped ZnO visible nano photocatalyst for removing of methylene blue, Journal of Materials Science: Materials in Electronics, 28 (2017) 5941-5952.

[46] P. Jakinala, H. Naik Lavudi, N. Angali, S. Ganderla, K.K. Inampudi, S. Balaji Andugulapati, M. Srinivas, M. Rao Katika, Green synthesis of ZnO-Ag nanocomposite using Stenotaphrum secundatum grass extract: Antibacterial activity and anticancer effect in oral squamous cell carcinoma CAL 27 cells, Inorganic Chemistry Communications, 152 (2023) 110735.

[47] M. Mehdi Zabihi, S. Eghbaliferiz, M. Khorashadizadeh, S. Mortazavi-Derazkola, M. Yousefi, Green synthesis of non-toxic silver nanoparticles using Salvia tebesana Bunge extract: Optimization, cytotoxicity, and antibacterial activities, Results in Chemistry, 7 (2024) 101510.

[48] R.K. Sali, M.S. Pujar, S. Patil, A.H. Sidarai, Green synthesis of ZnO and Ag-ZnO nanoparticles using macrotyloma uniflorum: evaluation of antibacterial activity, Adv. Mater. Lett, 12 (2021) 1-7.

[49] D. Thatikayala, V. Banothu, J. Kim, D.S. Shin, S. Vijayalakshmi, J. Park, Enhanced photocatalytic and antibacterial activity of ZnO/Ag nanostructure synthesized by Tamarindus indica pulp extract, Journal of Materials Science: Materials in Electronics, 31 (2020) 5324-5335.

[50] M.S. Khan, P.P. Dhavan, B.L. Jadhav, N.G. Shimpi, Ultrasound-Assisted Green Synthesis of Ag-Decorated ZnO Nanoparticles UsingExcoecaria agallochaLeaf Extract and Evaluation of Their Photocatalytic and Biological Activity, ChemistrySelect, 5 (2020) 12660-12671.

[51] Z. Noohpisheh, H. Amiri, S. Farhadi, A. Mohammadi-gholami, Green synthesis of Ag-ZnO nanocomposites using Trigonella foenum-graecum leaf extract and their antibacterial, antifungal, antioxidant and photocatalytic properties, Spectrochimica Acta Part A: Molecular and Biomolecular Spectroscopy, 240 (2020) 118595.

[52] Z. Kiani, H. Aramjoo, P. Mohammadparast, F. Bahraini, A. Yousefinia, P.U. Nguyen, M. Fattahi, S. Mortazavi-Derazkola, Green synthesis of LAE@ZnO/Ag nanoparticles: Unlocking the multifaceted potential for biomedical and environmental applications, Journal of Environmental Chemical Engineering, 11 (2023) 111045.

[53] S. Parmar, H. Kaur, J. Singh, A.S. Matharu, S. Ramakrishna, M. Bechelany, Recent Advances in Green Synthesis of Ag NPs for Extenuating Antimicrobial Resistance, Nanomaterials, 12 (2022) 1115.

[54] R. Razavi, M. Amiri, H.A. Alshamsi, T. Eslaminejad, M. Salavati-Niasari, Green synthesis of Ag nanoparticles in oil-in-water nano-emulsion and evaluation of their antibacterial and cytotoxic properties as well as molecular docking, Arabian Journal of Chemistry, 14 (2021) 103323.

[55] F.O. Al-Otibi, M.T. Yassin, A.A. Al-Askar, K. Maniah, Green Biofabrication of Silver Nanoparticles of Potential Synergistic Activity with Antibacterial and Antifungal Agents against Some Nosocomial Pathogens, Microorganisms, 11 (2023) 945.

[56] S.N.A. Mohamad Sukri, K. Shameli, S.-Y. Teow, J. Chew, L.-T. Ooi, M. Lee-Kiun Soon, N.A. Ismail, H. Moeini, Enhanced antibacterial and anticancer activities of plant extract mediated green synthesized zinc oxide-silver nanoparticles, Front Microbiol, 14 (2023) 1194292.

[57] P. Chaudhary, P. Janmeda, A.O. Docea, B. Yeskaliyeva, A.F. Abdull Razis, B. Modu, D. Calina, J. Sharifi-Rad, Oxidative stress, free radicals and antioxidants: Potential crosstalk in the pathophysiology of human diseases, Frontiers in chemistry, 11 (2023) 1158198.

[58] V.P. Reddy, Oxidative Stress in Health and Disease, Biomedicines, 11 (2023) 2925.

[59] A. García-Sánchez, A.G. Miranda-Díaz, E.G. Cardona-Muñoz, The Role of Oxidative Stress in Physiopathology and Pharmacological Treatment with Pro- and Antioxidant Properties in Chronic Diseases, Oxidative Medicine and Cellular Longevity, 2020 (2020) 2082145.

[60] F. Pourmorad, S. Hosseinimehr, N. Shahabimajd, Antioxidant activity, phenol and flavonoid contents of some selected Iranian medicinal plants, African journal of biotechnology, 5 (2006).

[61] B. Kędzierski, W. Kukula-Koch, J. Widelski, K. Głowniak, Impact of harvest time of Aesculus hippocastanum seeds on the composition, antioxidant capacity and total phenolic content, Industrial Crops and Products, 86 (2016) 68-72.

[62] Z. Bedlovičová, I. Strapáč, M. Baláž, A. Salayová, A Brief Overview on Antioxidant Activity Determination of Silver Nanoparticles, Molecules, 25 (2020) 3191.

[63] A.K. Keshari, R. Srivastava, P. Singh, V.B. Yadav, G. Nath, Antioxidant and antibacterial activity of silver nanoparticles synthesized by Cestrum nocturnum, Journal of Ayurveda and Integrative Medicine, 11 (2020) 37-44.

[64] S. Hameed, A.T. Khalil, M. Ali, M. Numan, S. Khamlich, Z.K. Shinwari, M. Maaza, Greener Synthesis of Zno and Ag–Zno Nanoparticles Using Silybum Marianum for Diverse Biomedical Applications, Nanomedicine, 14 (2019) 655-673.

[65] P. Suresh, A. Doss, R.P. Praveen Pole, M. Devika, Green synthesis, characterization and antioxidant activity of bimetallic (Ag-ZnO) nanoparticles using Capparis zeylanica leaf extract, Biomass Conversion and Biorefinery, 14 (2024) 16451-16459.

[66] M. Hosny, M. Fawzy, A.S. Eltaweil, Green synthesis of bimetallic Ag/ZnO@Biohar nanocomposite for photocatalytic degradation of tetracycline, antibacterial and antioxidant activities, Scientific Reports, 12 (2022) 7316.

[67] S. R, J.A. Jebasingh, M.V. S, P.K. Stanley, P. Ponmani, M.E. Shekinah, J. Vasanthi, Excellent Photocatalytic degradation of Methylene Blue, Rhodamine B and Methyl Orange dyes by Ag-ZnO nanocomposite under natural sunlight irradiation, Optik, 231 (2021) 166518.

[68] M. Ahmad, M.T. Qureshi, W. Rehman, N.H. Alotaibi, A. Gul, R.S. Abdel Hameed, M.A. Elaimi, M.F.H. Abd el-kader, M. Nawaz, R. Ullah, Enhanced photocatalytic degradation of RhB dye from aqueous solution by biogenic catalyst Ag@ZnO, Journal of Alloys and Compounds, 895 (2022) 162636.

Figure captions

Table.1. Antibacterial effects (MIC values in µg/mL) of *A. Hippocastanum* fruit extract, ZnONPs, and ZnO-Ag@*AHFE* NPs.

Table.2. Antioxidant activity results of *A. Hippocastanum* fruit extract, ZnONPs, and ZnO-Ag@*AHFE* NPs.

Scheme.1. Scheme of the proposed mechanism for the synthesis of ZnO-Ag@*AHFE* NPs

Fig.1. Process of green synthesis for ZnO-Ag@*AHFE* NPs generation.

Fig.2. XRD pattern of (a) ZnONPs and (b) ZnO-Ag@*AHFE* NPs.

Fig.3. FT-IR spectra of (a) ZnONPs and (b) ZnO-Ag@*AHFE* NPs.

Fig.4. TEM images of ZnO-Ag@*AHFE* NPs.

Fig.5. Bar graph comparing the MICs of ZnO and ZnO-Ag@*AHFE* NPs against different bacterial strains.

Fig.6. The proposed antibacterial mechanism of ZnO-Ag@*AHFE* NPs.

Fig.7. Degradation rates of rhodamine B and methylene blue dyes in the presence of ZnONPs under UV light.

Fig.8. Degradation rates of rhodamine B and methylene blue dyes in the presence of ZnO-Ag@*AHFE* NPs under UV light.

Table.1.

Strains	*A. hippocastanum* fruit extract	ZnO NPs	ZnO-Ag@*AHFE* NPs	Tetracycline
	MIC (µg/mL)	**MIC (µg/mL)**	**MIC (µg/mL)**	**MIC (µg/mL)**
E. coli (ATCC 25922)	>15000	2000	125	0.97
K. pneumoniae (ATCC 9997)	>15000	1000	250	7.8
P. aeruginosa (ATCC 27853)	>15000	4000	125	3.9
S. aureus (ATCC 25923)	>15000	500	250	0.97
E. faecalis (ATCC 29212)	15000	4000	750	7.8

Table.2.

Sample	Concentration (mg/mL)	Mean DPPH Inhibition ± SD (%)
ZnO NPs	4	8 ± 0.6
	2	3 ± 0.4
	1	2 ± 0.3
***A. hippocastanum* fruit extract**	4	35 ± 2.1
	2	20 ± 3.7
	1	8 ± 1.1
ZnO-Ag@*AHFE* NPs	2	85 ± 2.4
	1	62 ± 1.4
	0.5	42 ± 1.7

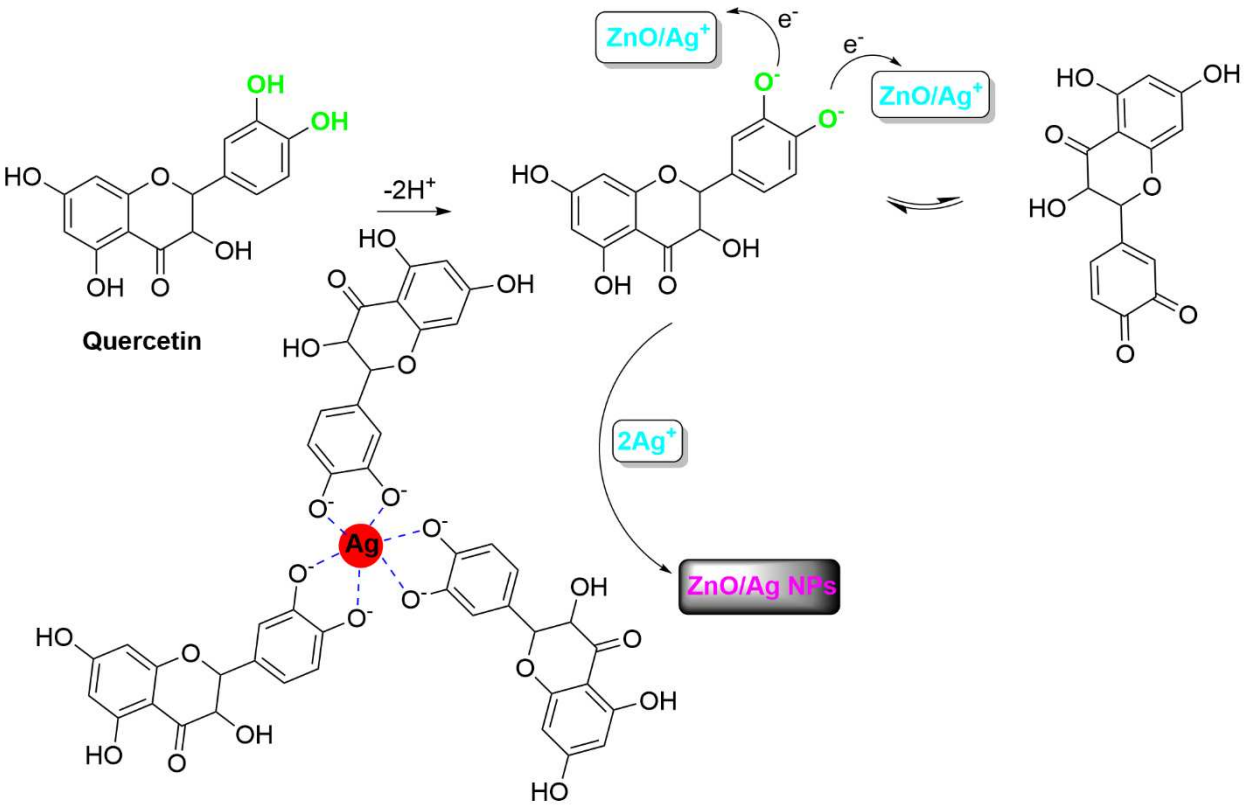

Scheme.1.

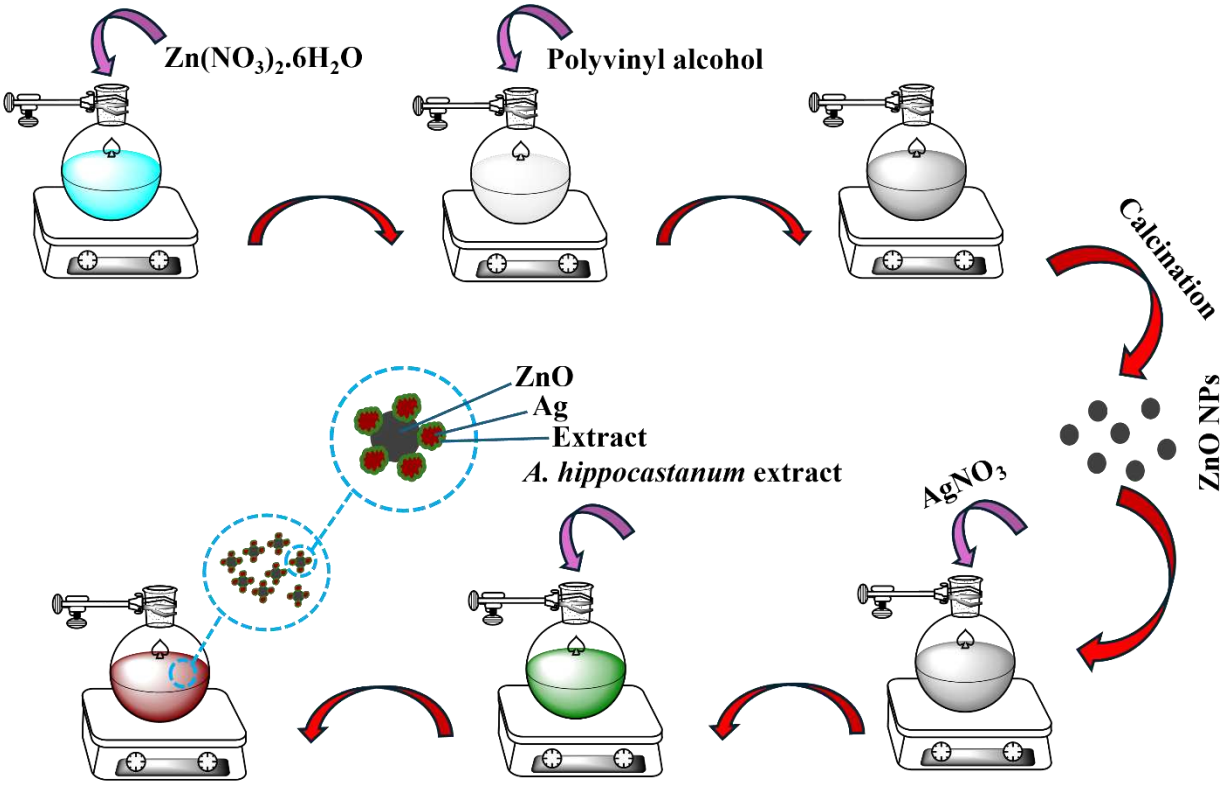
Zn(NO3)2.6H2O
Polyvinyl alcohol
Calcination
ZnO NPs
ZnO
Ag
Extract
A. hippocastanum extract
AgNO3

Fig.1.

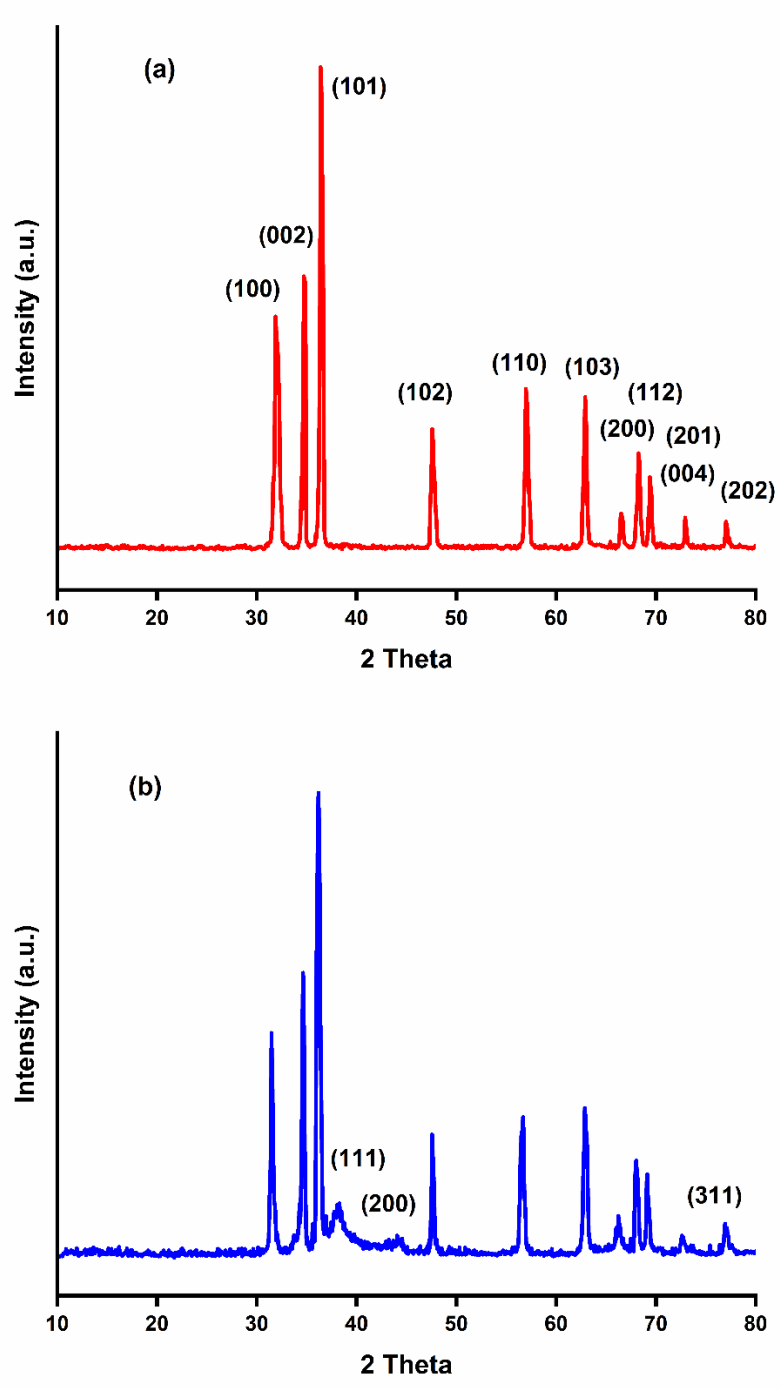
(a)
(101)
(002)
(100)
(102)
(110)
(103)
(112)
(200)
(201)
(004)
(202)
Intensity (a.u.)
10
20
30
40
50
60
70
80
2 Theta
(b)
(111)
(200)
(311)
Intensity (a.u.)
10
20
30
40
50
60
70
80
2 Theta

Fig.2.

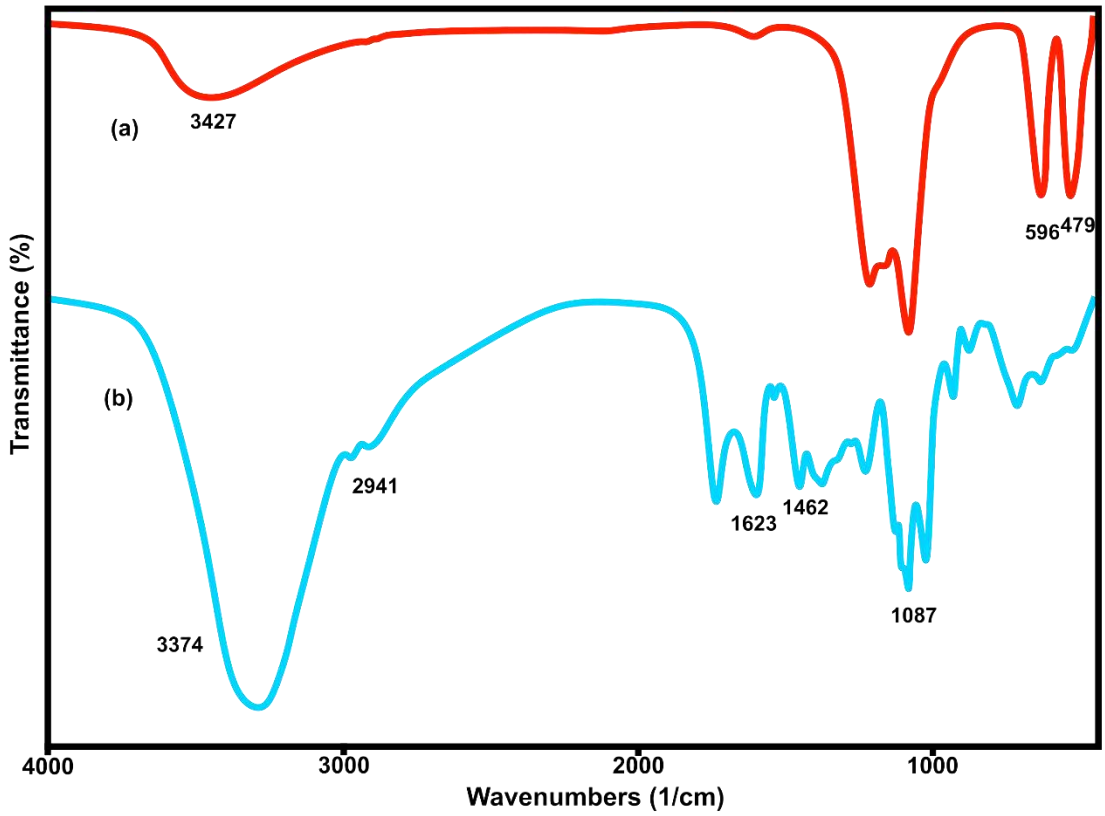
(a)
3427
596
479
(b)
2941
1623
1462
1087
3374
Transmittance (%)
4000
3000
2000
1000
Wavenumbers (1/cm)

Fig.3.

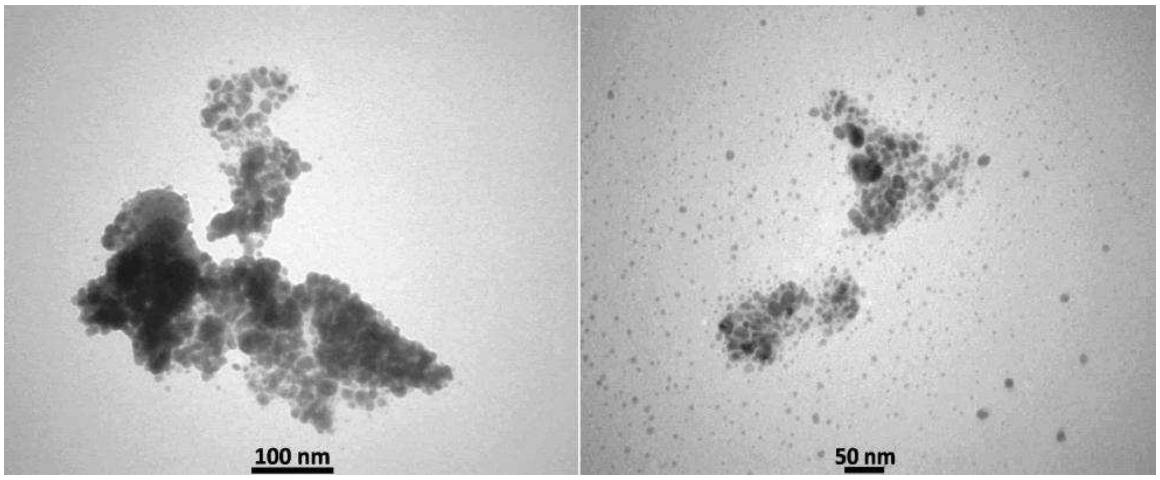

Fig.4.

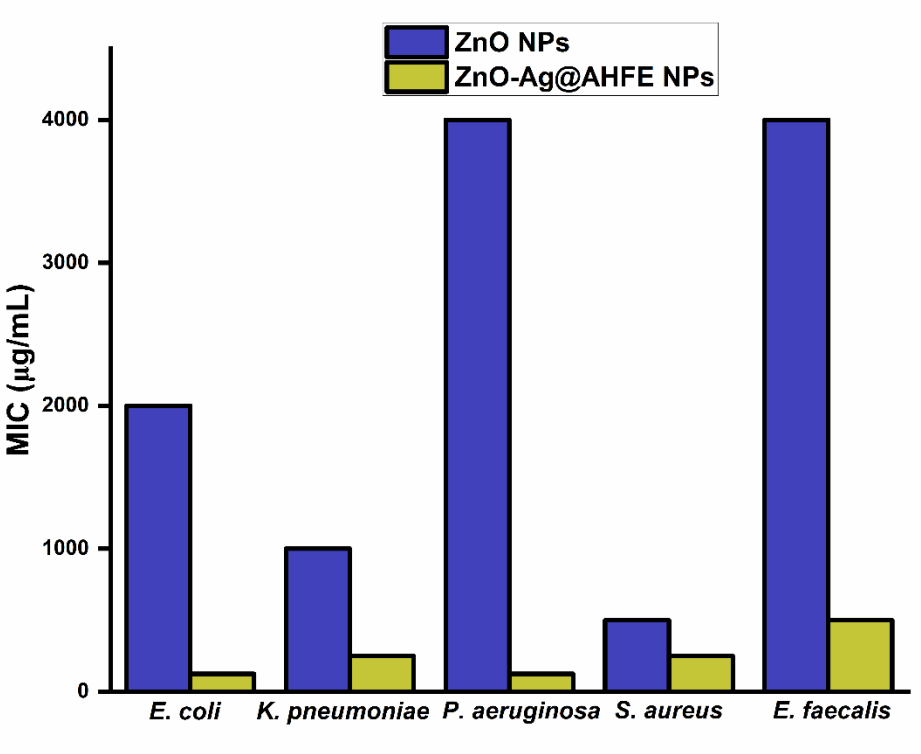
ZnO NPs
ZnO-Ag@AHFE NPs
MIC (μg/mL)
0
1000
2000
3000
4000
E. coli
K. pneumoniae
P. aeruginosa
S. aureus
E. faecalis

Fig.5.

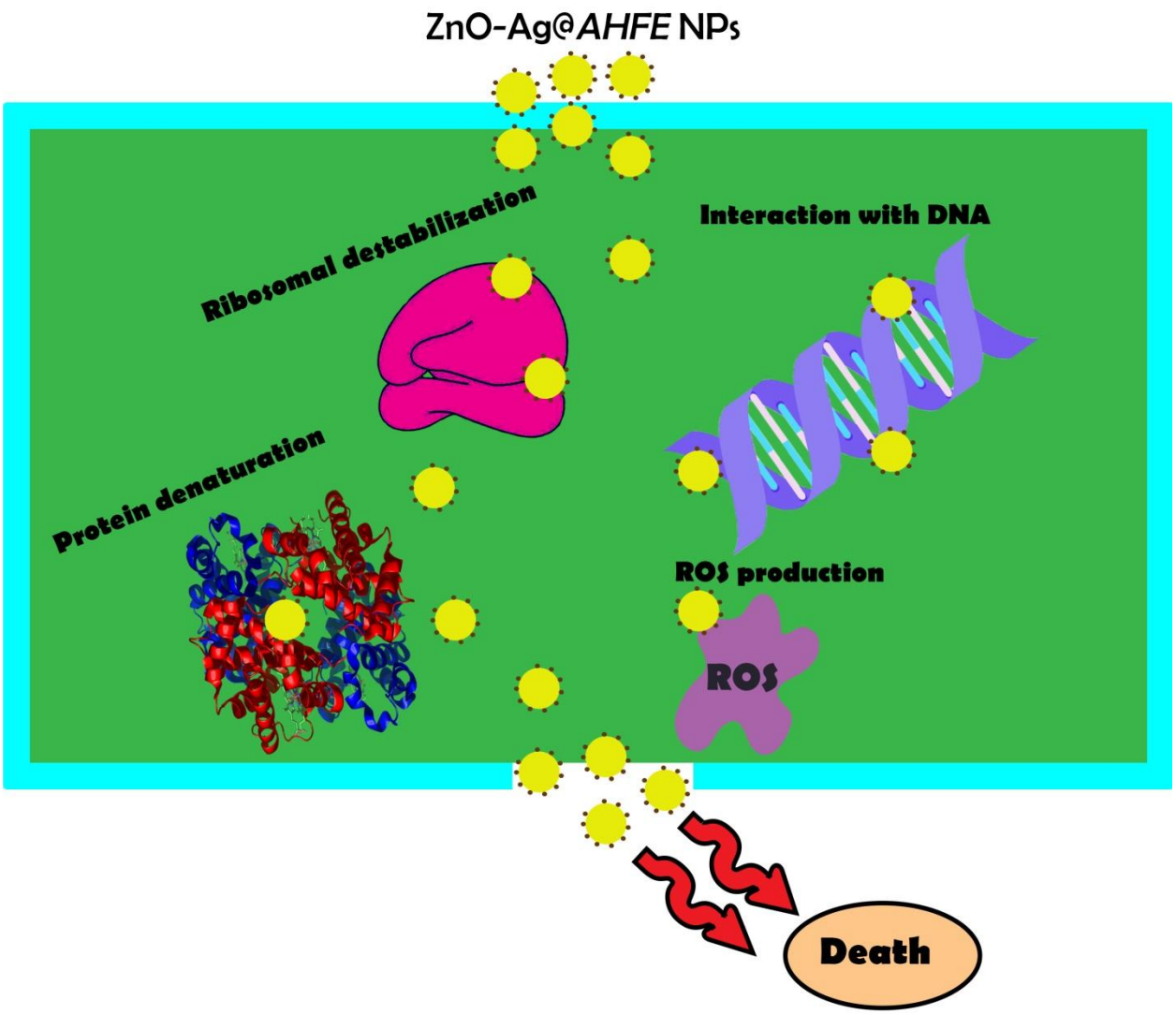
ZnO-Ag@AHFE NPs
Ribosomal destabilization
Interaction with DNA
Protein denaturation
ROS production
ROS
Death

Fig.6.

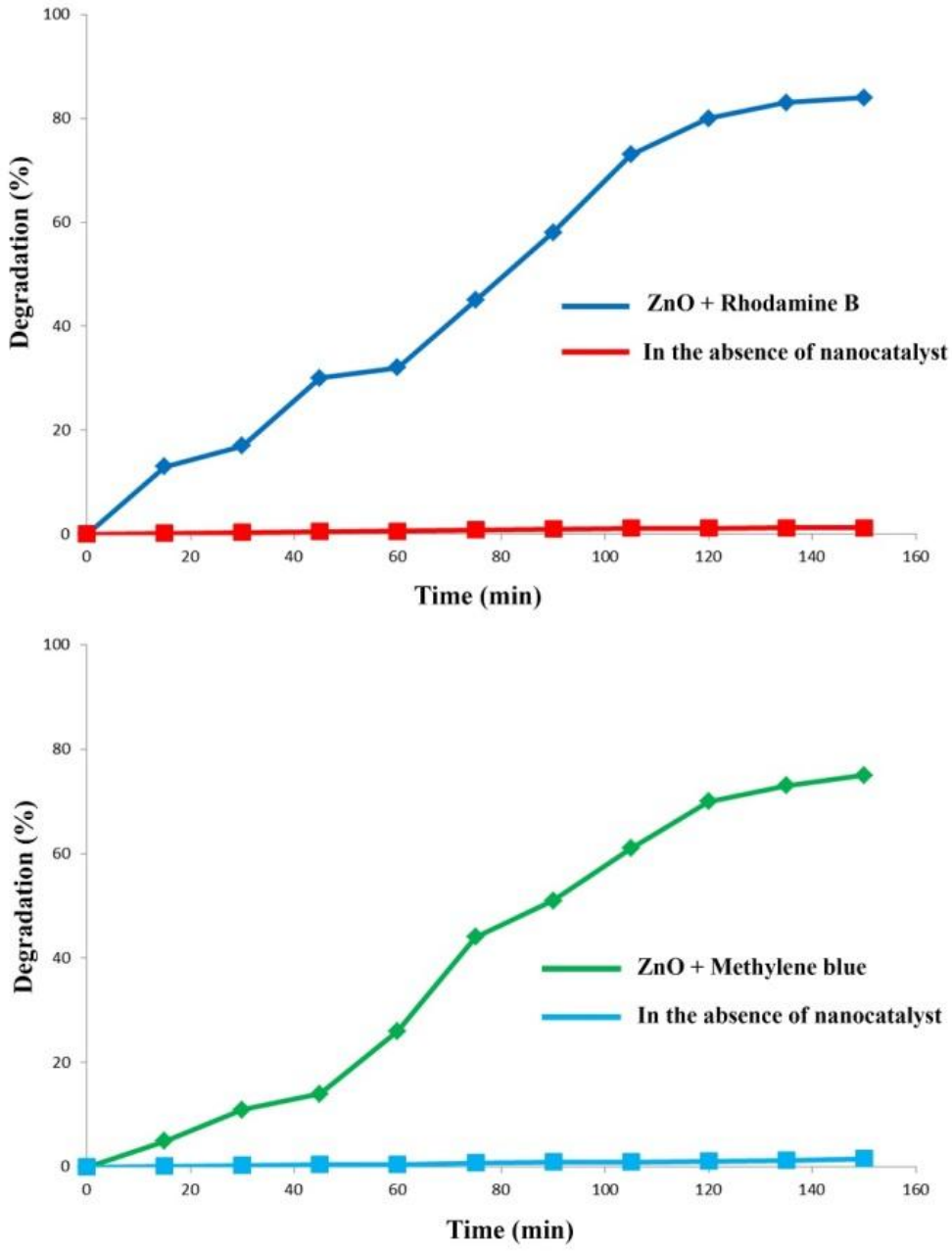
Degradation (%)
Time (min)
ZnO + Rhodamine B
In the absence of nanocatalyst
Degradation (%)
Time (min)
ZnO + Methylene blue
In the absence of nanocatalyst

Fig.7.

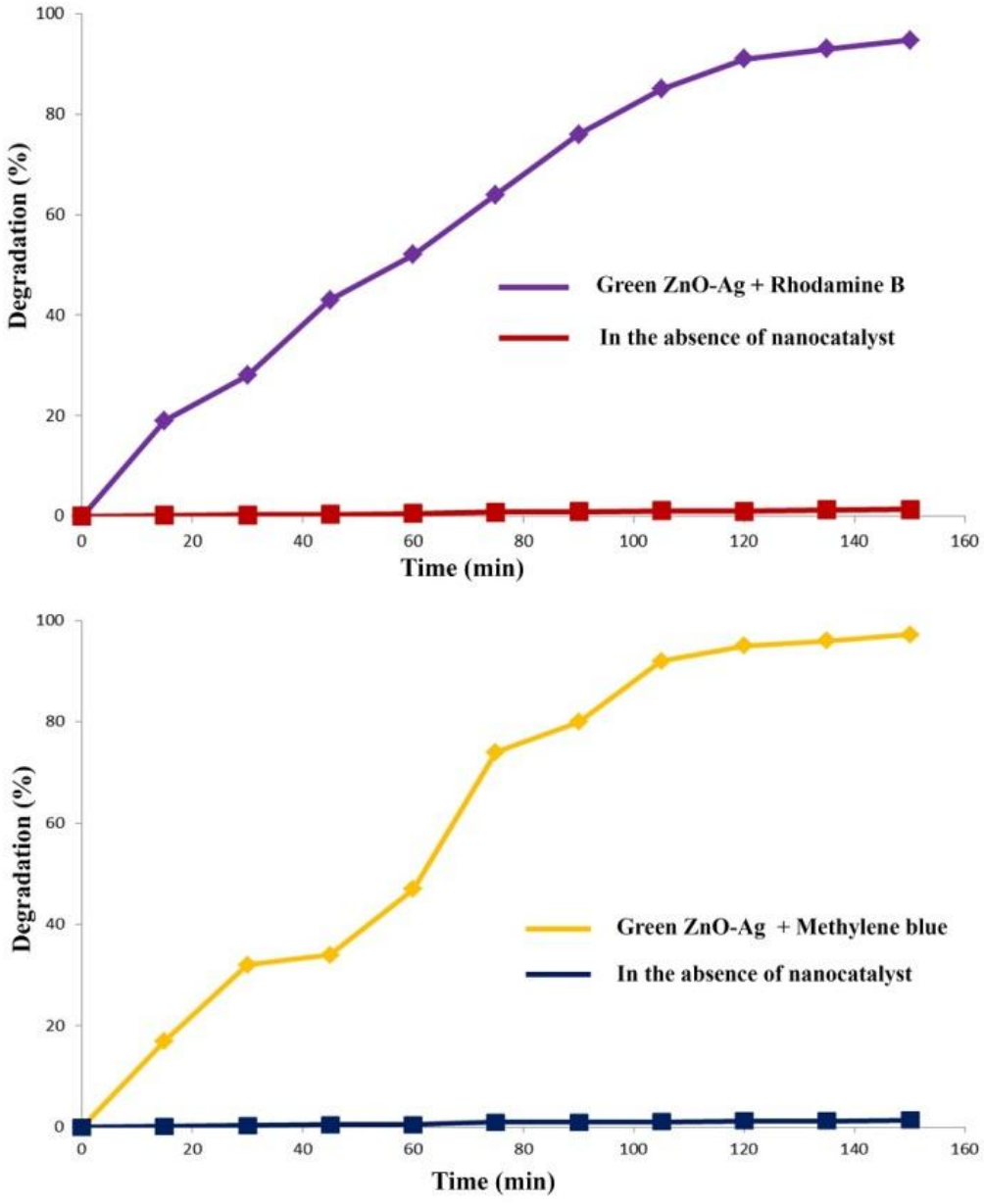
Degradation (%)
Time (min)
Green ZnO-Ag + Rhodamine B
In the absence of nanocatalyst
Degradation (%)
Time (min)
Green ZnO-Ag + Methylene blue
In the absence of nanocatalyst

Fig.8.